Two-Photon Laser Microprinting of Highly Ordered Nanoporous Materials Based on Hexagonal Columnar Liquid Crystals

Joël Monti [a], *Alberto Concellón* [b], *Ruiqi Dong* [c], *Mira Simmler* [d], *Alexander Münchinger* [e], *Christian Huck* [f], *Petra Tegeder* [f], *Hermann Nirchl* [d], *Martin Wegener* [a, e], *Chinedum Osuji* [c], *Eva Blasco* [a, g] *

[a] *Institute of Nanotechnology (INT), Karlsruhe Institute of Technology (KIT), 76344 Eggenstein-Leopoldshafen, Germany*

[b] *Department of Chemistry, Massachusetts Institute of Technology (MIT), Cambridge, MA 02139, USA*

[c] *Department of Chemical and Biomolecular Engineering, the University of Pennsylvania, Philadelphia, PA 19104, USA*

[d] *Institute of Mechanical Process Engineering and Mechanics (MVM), Karlsruhe Institute of Technology (KIT), 76131 Karlsruhe, Germany*

[e] *Institute of Applied Physics (APH), Karlsruhe Institute of Technology (KIT), 76131 Karlsruhe, Germany*

[f] *Institute of Physical Chemistry, Heidelberg University, 69120 Heidelberg, Germany*

[g] *Center for Advanced Materials (CAM), Heidelberg University, 69120 Heidelberg, Germany*

* Email: eva.blasco@oci.uni-heidelberg.de

Two-photon printing– Nanoporous columnar liquid crystal – Self-assembly – Selective adsorption

ABSTRACT

Nanoporous materials relying on supramolecular liquid crystals (LCs) are excellent candidates for size- and charge- selective membranes. However, whether they can be manufactured using printing technologies remained unexplored so far. In this work, we develop a new approach for the fabrication of ordered nanoporous microstructures based on supramolecular LCs using two-photon laser printing. In particular, we employ photo-cross-linkable hydrogen-bonded complexes, that self-assemble into columnar hexagonal (Col_h) mesophases, as the base of our printable photoresist. The presence of photopolymerizable groups in the periphery of the molecules enables the printability using a laser. We demonstrate the conservation of the Col_h arrangement and of the adsorptive properties of the materials after laser microprinting, which highlights the potential of the approach for the fabrication of functional nanoporous structures with a defined geometry. This first example of printable Col_h LC should open new opportunities for the fabrication of functional porous micro-devices with potential application in catalysis, filtration, separation, or molecular recognition.

INTRODUCTION

The development of new functional printable materials as well as 3D printing technologies, has transformative potential in a variety of fields such as optics and photonics,[1-5] bio-engineering[6-9], (micro)robotics,[10-13] and many more.[14-18] Among those functional materials, liquid crystals (LCs) have been widely explored due to their intrinsic anisotropy as well as their stimuli-responsive and self-healing properties.[19, 20] Within the vast variety of LCs, nematic LCs (NLCs) consisting of rod-shaped LC molecules have been extensively exploited over the last few decades: from LC displays (LCDs) to stimuli-responsive devices such as actuators, and more recently in 3D/4D printing.[21-24]

In particular, NLC-based materials have been successfully printed using different technologies including direct ink writing (DIW),[25-27] fused deposition modelling (FDM),[28, 29] inkjet printing,[30, 31] and very recently, employing two-photon 3D laser printing. 3D laser printing (also known as direct laser writing) has been established as an excellent tool for the fabrication of functional objects down to sub-micron resolution.[32, 33] Recent works using this technology have demonstrated the potential of NLCs for application in tunable microoptics[34,35] or as microscopic actuators.[36-39]

Columnar LCs are a different yet prominent class of LCs that is based on the self-assembly of discotic molecules into linear columnar stacks, by supramolecular interactions, such as π-π stacking, van der Waals interactions, or phase segregation.[40] The two-dimensional arrangement of the columnar self-assemblies results in hexagonal (Col_h), oblique, tetragonal or rectangular columnar mesophases.[41, 42] Typical designs of discotic molecules consist of a rigid core based on π-systems,[43, 44] substituted with flexible side chains that promote the formation of LC mesophases by disfavoring crystalline aggregation and favoring molecular mobility.[42 45-48] The introduction of terminal cross-linkable groups on the side chains enables fixation of the LC arrangement to produce polymer networks with highly anisotropic optical, thermal, and mechanical properties. These self-assembled LC networks have been used to construct a variety of functional materials, including ion-conductive membranes, chiro-optical elements, or nanoporous polymers.

Nanoporous responsive structures with relatively small pore dimensions (ca. 1 nm) have been prepared by using both lyotropic and thermotropic LCs.[49, 50] Nanopores are generally introduced in the LC material after the cross-linking process, and the morphology of the nanopores depends on the LC phase (e.g., columnar, smectic, or bicontinuous phases yield 1D, 2D or 3D pore geometries, respectively). The first example of a porous material based on columnar LCs was reported by Kim and coworkers,[51] and since then, several research groups started to investigate

these promising materials. A very common strategy is based on two complementary building blocks that are capable of interacting through H-bonding.[52-59] One of the components is a LC molecule bearing cross-linkable groups, whereas the other serves as template. Fixation of the LC molecular order via cross-linking is followed by template removal, which leads to porous materials with pore sizes comparable to that of the template. In fact, LC porous materials have recently shown remarkable capabilities as specific adsorbers or as nanofiltration membranes for water treatment.[56, 60] Despite the unique properties, diversity and versatility of LC porous materials, no reports on the printing of this kind of LC materials have been published to date. All the examples above are being mainly processed in films and are therefore, limited to planar and simple geometries (2D). Being able to print these functional nanoporous materials will allow for the manufacturing in unprecedented 3D shapes, which can be easily adapted on demand depending on the needs.

Thus, in an attempt to expand the state-of-the-art of nanoporous LC materials, we present here a new approach to access highly ordered porous microstructures with designed frameworks and functionalities by using two-photon laser printing. In particular, we employed discotic LC molecules based on H-bonded complexes, which consist of an aromatic core acting as a template and three peripheral benzoic acids (Figure 1). The surrounding tripodic acids were designed with three aliphatic side chains containing terminal acrylates as photo-cross-linkable units for laser printing. We demonstrate that the self-assembled LC materials exhibit Col_h mesophases and can be processed into shape-defined microstructures through laser-induced cross-linking of the peripheral acrylate moieties. Importantly, the LC ordering is retained during the manufacturing process. Chemical treatment allows the removal of the templating core from the cross-linked material via H-bonds breakage. Furthermore, we highlight the selective adsorptive properties of

the printed microstructures. Overall, our results illustrate that the ability to fabricate highly ordered porous microstructures with defined geometries can open new opportunities for the engineering of functional microdevices that enable selective adsorption.

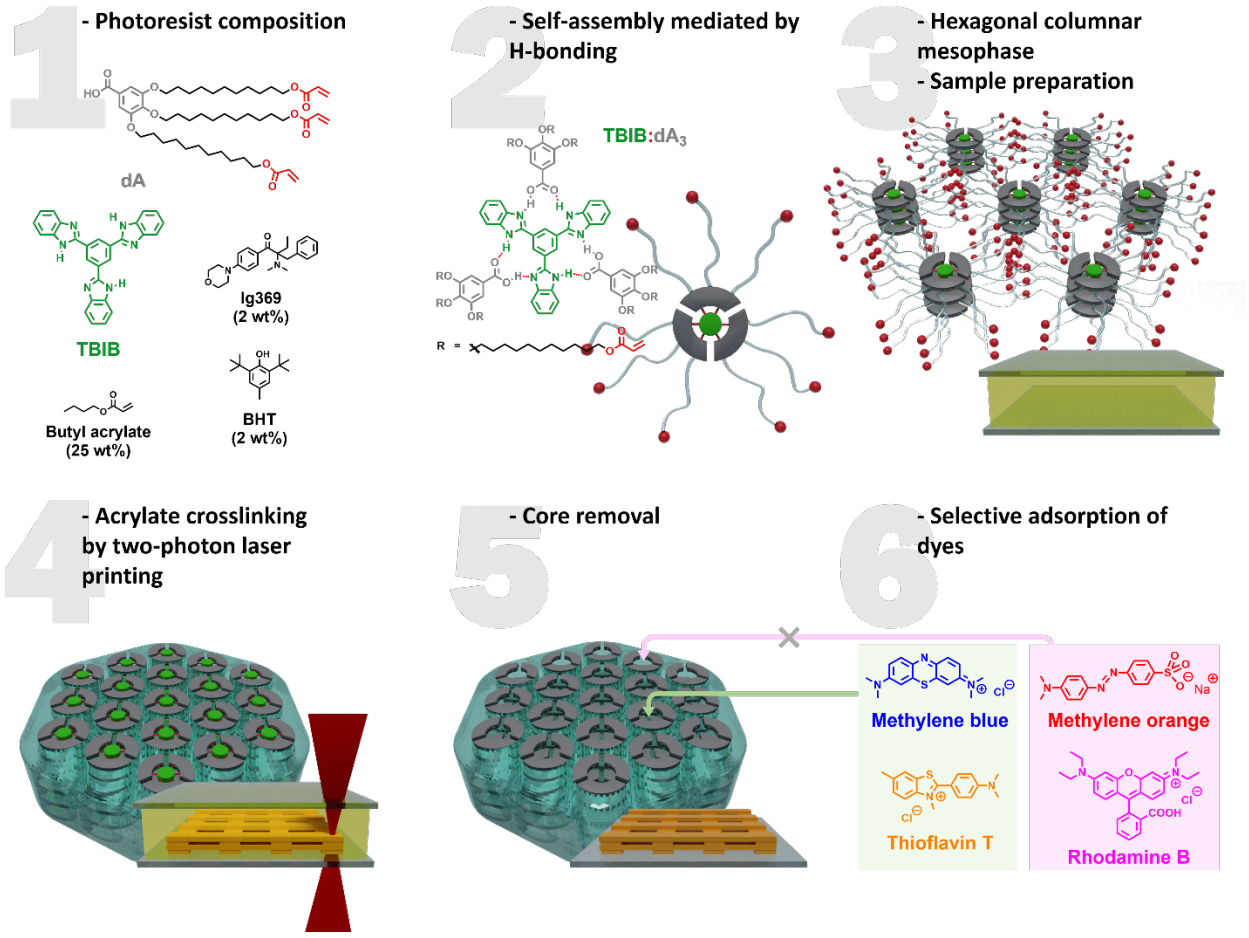

Figure 1. Schematic representation of the fabrication of a nanoporous microstructure by two-photon laser printing employing a hexagonal columnar (Col_h) LC photoresist. **(1)** Chemical structures of the cross-linker (**dA**), the templating core (**TBIB**), the photoinitiator (Ig369), the additive (butyl acrylate) and the radical scavenger (BHT) used in the system. **(2)** Chemical structure and schematic representation of the complex **TBIB:dA$_3$**, formed by H-bonding (red rods) of three **dA** (grey, the terminal acrylate groups are represented by red spheres) around a templating core **TBIB** (green). **(3)** Formation of a hexagonal columnar mesophase in-between two glass

slides. **(4)** Two-photon laser printing via photo-cross-linking of the terminal acrylate groups. Upon cross-linking, the arrangement of the Col_h mesophase is locked. **(5)** Core removal by H-bonding breakage. **(6)** The effective size of the pores as well as the effective charge allow for selective adsorption of chemical species.

RESULTS AND DISCUSSION

Design, synthesis, formulation and characterization of the columnar hexagonal (Col_h) printable system

The identification of a columnar LC system suitable for two-photon laser printing was a crucial first step. In particular, we selected photo-cross-linkable columnar hexagonal (Col_h) H-bonded complexes as suitable candidates. As mentioned above, H-bonded Col_h LCs possess the inherent ability to self-assemble into mesophases generating highly ordered porous materials by the removal of the core. The presence of photopolymerizable groups at the periphery enables the locking of the Col_h arrangement, and importantly for this work, they are essential for the fabrication of microstructures by laser printing. In order to circumvent competitive light absorption from the core, typical extended polyaromatic cores were rejected. Instead, we utilize three different templating cores, melamine (**M**), tris(triazolyl)triazine (**T**) and 1,3,5-tris(1H-benzo[d]imidazol-2-yl)benzene (**TBIB**). Also, a gallic acid derivative (**dA**) was decorated with three acrylate-terminated aliphatic chains, providing the final 3:1 complexes with a high degree of functionalization (nine acrylate groups per discotic molecule). This allows the formation of a strong matrix, by laser polymerization, without the aid of a secondary cross-linker.

The H-bonded complexes were prepared by mixing the core (**TBIB**, **T** or **M**) and the acid (**dA**) in a 1:3.1 ratio (detailed procedures are available in the supplementary information). A small

excess of **dA** was used to favor the formation of the 1:3 complex with respect to assemblies with lower **dA** content (1:1 or 1:2). The formation of the H-bonded assemblies was evidenced by ^{1}H-NMR and FTIR.[58] By ^{1}H-NMR, the down-field shifting of the proton signals in proximity to the carboxylic acid supported the formation of H-bonds with the corresponding core (Figure S1 in the supplementary information). **Figure 2** depicts an exemplary FTIR analysis for the formation of **TBIB:dA$_3$**. The formation of the assembly induced a shift of the C=O stretch band (1679 cm^{-1} to 1673 cm^{-1}) from the carboxylic acid moiety of **dA**. The C=O stretch band at 1729 cm^{-1} was attributed to the ester of the acrylate moiety. The appearance of an ionic-like N^{+}–H signal at 3254 cm^{-1} wavenumber also supported the formation of the H-bond assembly, in agreement with a previous study.[53]

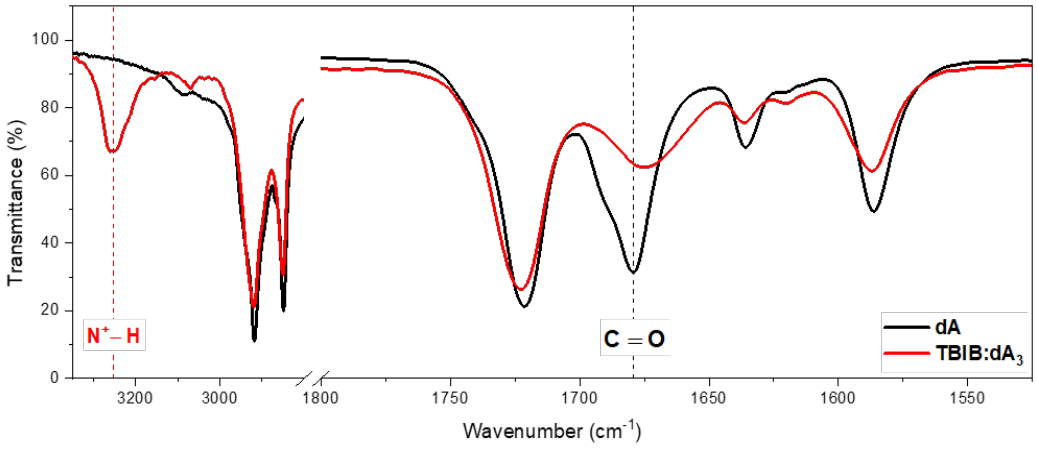

Figure 2. Analysis of the formation of **TBIB:dA$_3$** by FTIR. The shifts of the C=O stretch band of the benzoic acid moieties of **dA**, as well as the appearance of a N^{+}–H band corresponding to the H-bonded **TBIB** core support the formation of the assembly.

The LC behavior of all the complexes was studied by temperature-resolved polarized-light optical microscopy (POM). First, we carried out POM studies by heating the material to its isotropic state, and then slowly cooling it down to the Col$_h$ phase. **TBIB:dA$_3$** showed well-defined

conical and fan-shaped textures typical from columnar mesophases and a clearing point at about 170 °C. Nonetheless, the **M**- and **T**-containing complexes (**M:dA$_3$** and **T:dA$_3$**) exhibited less well-defined textures with small domains and less reproducible LC properties (Figures S12-S13). Based on these results, we decided to focus on the **TBIB:dA$_3$** complex for the formulation of Col_h photoresists.

In order to use **TBIB:dA$_3$** for two-photon laser printing, we prepared a photoresist including **TBIB:dA$_3$** as the main component, a photoinitiator, Irgacure 369 (Ig369) (2 wt%) as well as a radical scavenger, BHT (2 wt%). The use of a scavenger serves the double purpose to limit the undesired thermal cross-linking of acrylates during the thermal treatments, as well as to widen the parameters space that allows printing of the material. As mentioned before, **TBIB:dA$_3$** exhibited a clearing point at around 170 °C, which did result in significant pre-polymerization of the resist during the thermal treatment for the mesophase formation. Thus, 25 wt% of butylacrylate (BuA) was incorporated to lower the clearing point of the photoresist and limit unintended thermal pre-polymerization;[78] in particular, the clearing point of the photoresist decreased from 170 °C to about 100 °C. Importantly, POM studies of the photoresist also showed the formation of LC textures characteristic of Col_h mesophases (Figure 3a).

To further characterize the LC arrangement in the **TBIB:dA$_3$** photoresist formulation, as well as the impact of the photo-cross-linking on this arrangement, both the non-cross-linked photoresist and cross-linked films were analyzed by wide-angle X-Ray scattering (WAXS) (Figure 3b). Cross-linked films of 16 μm thickness were prepared by UV-irradiation (390−395 nm, 900 mW) of thermally treated Col_h photoresists for 3 min, and analyzed as free-standing films. Our WAXS results supported the previous POM observations for the assembly of **TBIB:dA$_3$** into a Col_h mesophase. For the photoresist, the WAXS patterns exhibited peaks with a ratio of their associated

q-values of q^*, $\sqrt{3}\,q^*$, $\sqrt{4}\,q^*$ and $\sqrt{7}\,q^*$ in the low-angle region (Figure 3c), which corresponded to the (100), (110), (200) and (210) reflections of a Col_h arrangement with a lattice constant of a = 3.96 nm. The obtained value for the inter-columnar distance is in good agreement with previous reports.[56, 61] For the photo-cross-linked films, the ratio of the q-values for the small-angle reflection peaks and the inter-columnar distance (a = 4.02 nm) were retained, which indicates the effective conservation of the Col_h arrangement during the photo-cross-linking process (Figure 3b). In both cases, in the wide-angle region, we observed two broad peaks corresponding to the π—π stacking of the aromatic cores (0.35 nm) and to the liquid-like correlations of the aliphatic chains (0.45 nm).

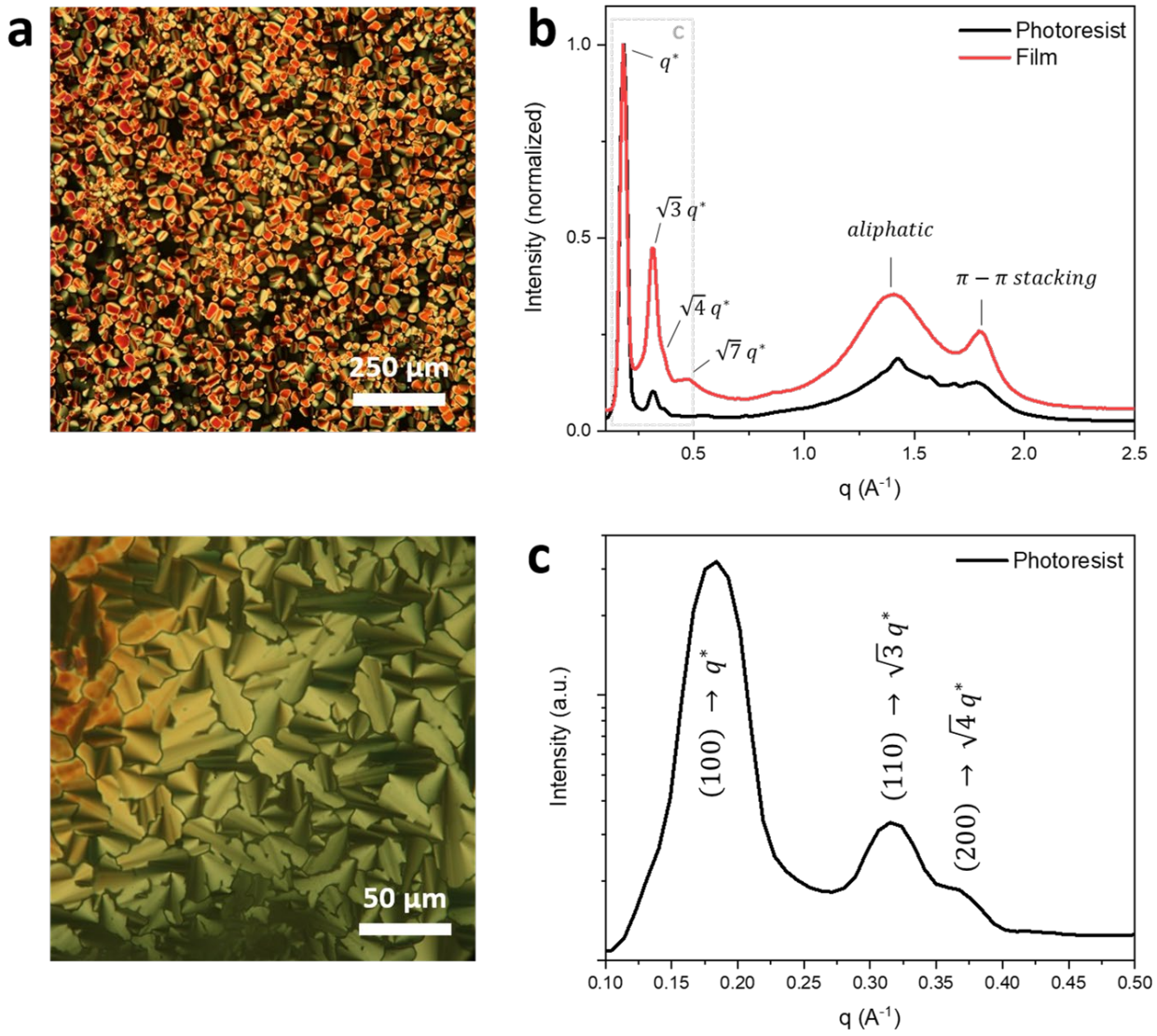

Figure 3. Characterization of the Col_h phase of the **TBIB:dA$_3$** photoresist. **(a)** Two examples of LC textures observed by POM. **(b)** WAXS data for **TBIB:dA$_3$** as non-cross-linked photoresist (black) and as a cross-linked film (red). **(c)** Main peaks in the small-angle region for the non-cross-linked photoresists.

Two-photon laser printing of Col_h photoresists

Once fully characterized, the **TBIB:dA$_3$** photoresist was investigated for microprinting using a commercially available two-photon laser printer (Photonics Professional GT, Nanoscribe GmbH).

Sandwich cells were prepared with one of the glass slides being functionalized with methacrylate groups. The functionalization of the glass substrate allows the covalent binding of the printed microstructures onto the substrate, and thus avoids the detachment of the structures during development. The microprinting was performed using an objective with a 25x magnification and a numerical aperture of NA = 0.8. The sandwiched self-assembled photoresist layer was printed in immersion-oil configuration, that is, printed on the first glass slide through which the laser light impinges. This method was chosen to reduce the negative effect of the LC birefringence and the translucency of the photoresist (which would otherwise lead to two laser foci), by minimizing the path length of the laser beam within the Col_h material.

The printing parameters were optimized based on high scanning speeds of 20 mm s^{-1} and 25 mm s^{-1}. With these scanning speed, laser powers of 20 mW and 25 mW, respectively, were determined to be the best suited. In each case, the minimal laser power leading to a sufficient cross-linking to allow the shape retention of the structures was chosen. Indeed, high doses resulted in the alteration of the properties of the material and/or to the deterioration of the material by overexposure and/or micro-explosions. In order to demonstrate the versatility of the technique, we designed different 2.5D geometries for laser printing, including simple patterns such as hexagons with holes or detailed finer patterns such as a map of the world, or a representation of the inner circle in Karlsruhe (Germany) (Figure 4 and S11). More complex (2.5D+) shapes containing voids, such as a cubic packing of rods, were also tested. The microprinted structures were developed in a $CHCl_3$:MeOH mixture similar to the mixture used for the self-assembly of **TBIB:dA$_3$**.

When printing at optimal conditions, the stability of the Col_h mesophase, related to the fairly high clearing point of the photoresist, was shown to be advantageous as it prevented the local thermal disruption of the mesophase, thus widening printing opportunities and increasing its

reliability. POM imaging of the printed structures showed the retention of the LC textures, supporting the retention of the Col_h arrangement in the cross-linked material. Moreover, the scanning electron microscopy (SEM) imaging of the microstructures confirmed the quality of the printed 2.5D microstructures, showing good definition, sharp edges and straight surfaces, as well as low shrinkage after development. The fabrication of structures of increasing heights showed an increasingly significant loss of definition for thickened structures, with a threshold of about 30 µm. This loss of definition was attributed to the birefringence of the LC material. Including 3D features such as voids or overhanging parts evidenced some limitations related to the proximity effect, maximal achievable definition and height constraints. Nonetheless, we are confident that more transparent microscopically ordered Col_h materials can decrease the height constraints, and enable the printing of more elaborated 3D structures in the future.

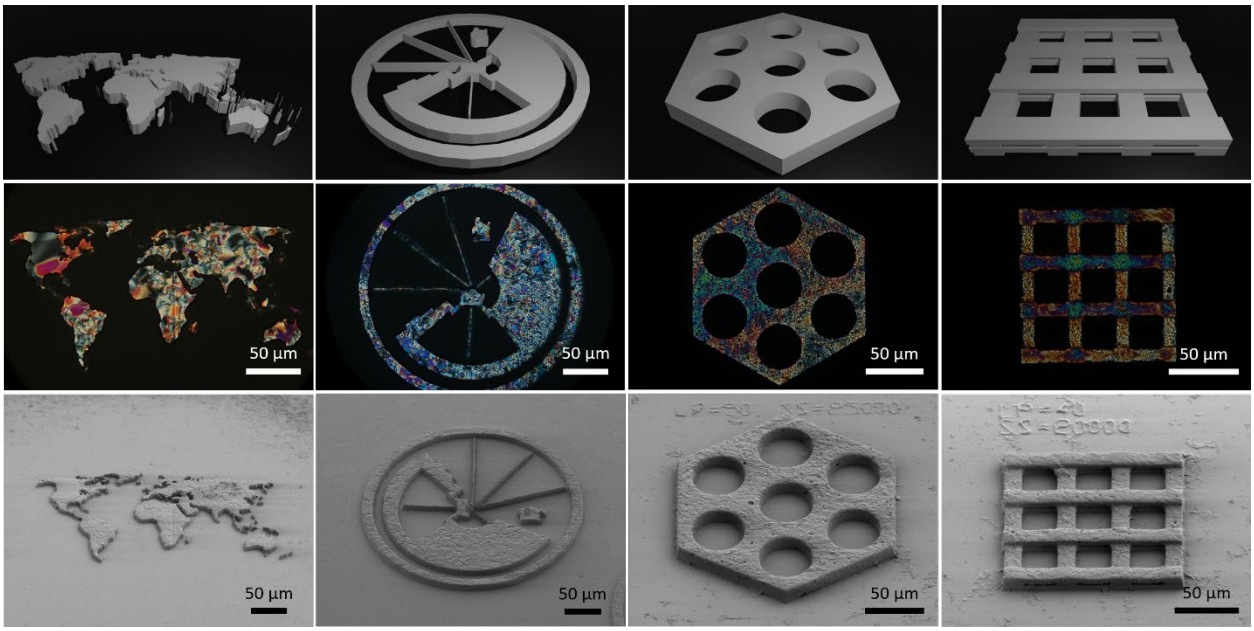

Figure 4. Models (top), POM image (middle) and SEM images (bottom) of four different microprinted structures. From left to right, a map of the world, a representation of the inner circle in Karlsruhe, a hexagon with holes and a cubic stack of rods.

Nanoporous microstructures formation by the removal of the templates

Ordered nanoporous materials were created by the removal of the templating core from the **TBIB:dA$_3$** complexes, for both printed microstructure and photo-cross-linked films as reference macroscopic material. The design of Col_h material **TBIB:dA$_3$** relies on H-bonding, and thus the template can be removed by chemical treatment in 0.1 wt% NaOH in dimethylsulfoxide (DMSO).[55] Since **dA** is a benzoic acid, the obtained pores are functionalized with anionic benzoate moieties after core removal with 0.1 wt% NaOH in DMSO. In a second step, the charge of the pores can be neutralized by protonation of the benzoate moieties with HCl (1 N).

First, FTIR spectroscopy was used to monitor the template removal of the macroscopic photo-cross-linked films and compared with the printed macrostructures. As it can be seen in the spectra depicted in Figure 5a, after basic treatment, the C=O band for the H-bonded benzoic acids of **TBIB:dA$_3$** shifted to an asymmetric C=O stretching band at 1565 cm^{-1}, and the band for **TBIB** as part of the H-bond assembly (3254 cm^{-1}) was lost. The results were in agreement with literature,[53] and thus evidenced the removal of the **TBIB** core. In the case of the microscopic samples, we employed FTIR microscopy to monitor the process. This technique allowed us to measure the FTIR spectra of the small printed specimens, in particular, cuboid microstructure (250 × 250 × 9.5 μm^3). The same changes in the C=O and N^+─H bands were observed for the microstructures, confirming the effective removal of the template (Figure 5b). Also, it was observed that, due to size scale difference, the core removal from microprinted structures was achieved upon exposure to the DMSO solution from 3 min to 10 min, while films required an exposure of several hours to afford a complete removal of the **TBIB** core (Figure S10). Additionally, the preservation of the LC order after core removal of photo-cross-linked films was proved by WAXS. The q^*, $\sqrt{3}\,q^*$, $\sqrt{4}\,q^*$ and $\sqrt{7}\,q^*$ ratio for the (100), (110), (200) and (210)

reflections in the small-angle region (Figure 5d) demonstrated the conservation of the Col_h arrangement and importantly, a consistent inter-columnar spacing was found. The finding of a conserved LC arrangement upon core removal was in agreement with previous reports of similar systems.[51, 58, 62]

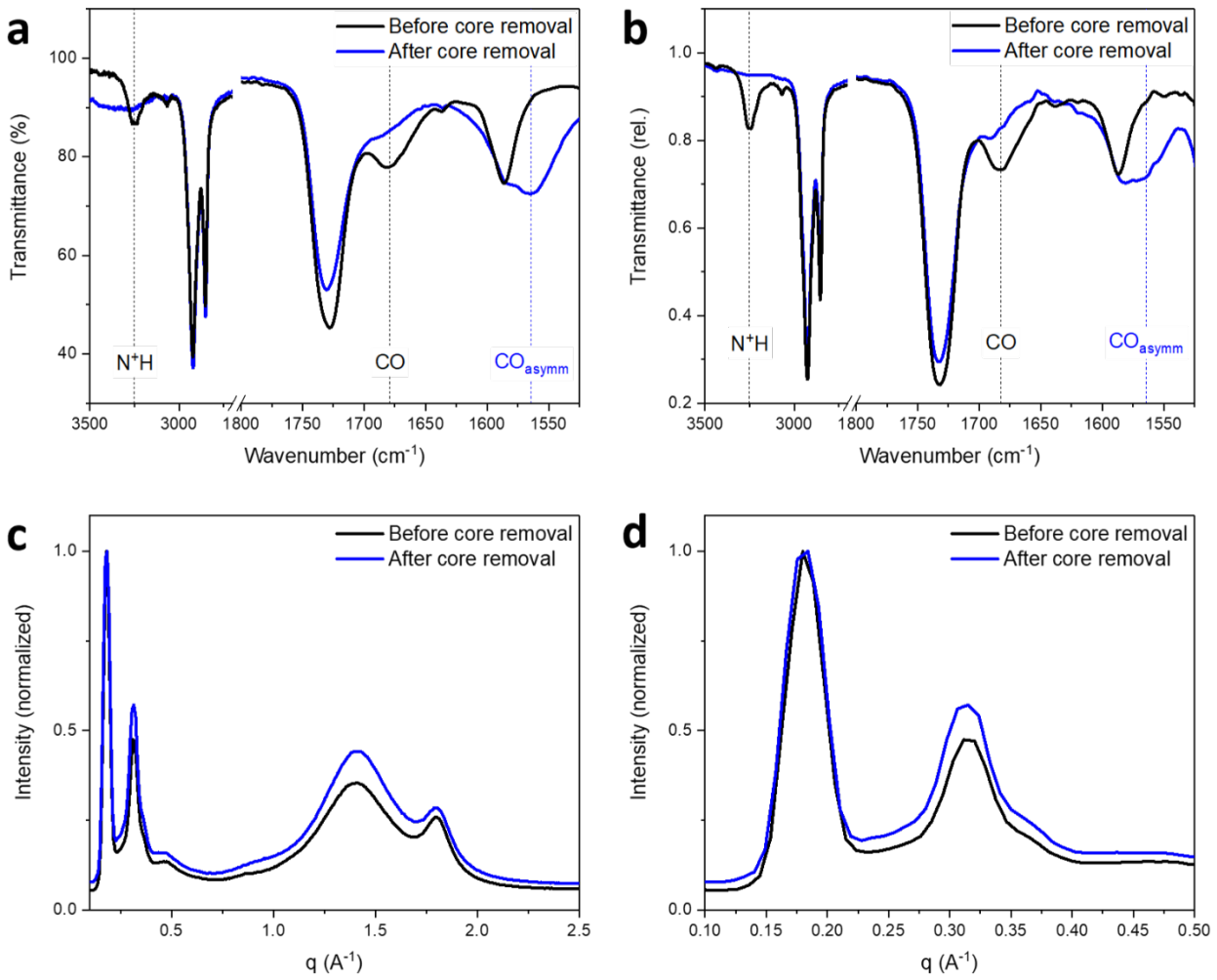

Figure 5. Analysis of photo-cross-linked **TBIB:dA$_3$** before (black) and after (blue) the removal of the **TBIB** core in 0.1 wt% NaOH in DMSO. FTIR spectra for **(a)** a film obtained by UV irradiation for 3 minutes, and **(b)** a microstructure fabricated by two-photon printing. WAXS data for **(c)** a photo-cross-linked film, and **(d)** zoom in the low-angle region of the spectra. WAXS data are normalized for easier comparison.

Selective Adsorption of Dyes

Finally, studies of the adsorptive properties of the porous material were carried out using four different dyes: methylene blue, thioflavin T, methylene orange and rhodamine B.[58, 61] After core removal with 0.1 wt% NaOH in DMSO, the obtained nanoporous material was negatively charged. It is thus expected to allow the adsorption of small cationic molecules such as methylene blue and thioflavin T. However, the structures should be less permeable to anionic molecules (methylene orange) or sufficiently large molecules (rhodamine B) due to electrostatic repulsion (Donan exclusion) and size-exclusion, respectively. For printed microstructures fabricated by two-photon printing, by optical microscopy, we observed a strong coloration of the microstructures treated with methylene blue and thioflavin T. Furthermore, the homogeneous and dense adsorption of methylene blue within the pores of the entire bulk of microstructures produced by two-photon laser printing, was evidenced by fluorescence confocal microscopy. On the other hand, the microstructures treated with methylene orange or rhodamine B exhibited little to no coloration, indicating little uptake of the dyes (Figure 6). The minimal coloration of these samples was attributed to the deposition of the dyes at the surface of the microstructures.

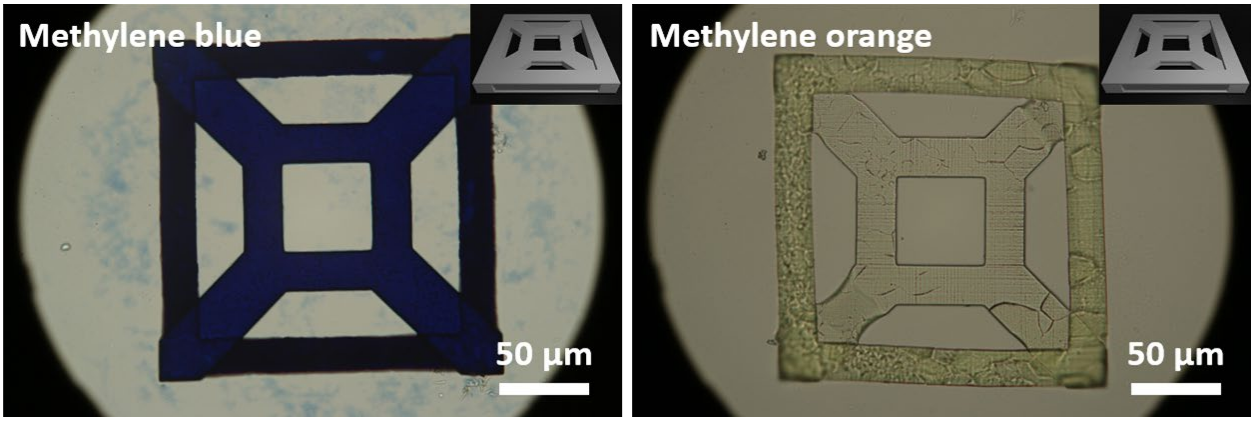

Figure 6. Optical microscopy images of microstructures after core removal and exposure to a solution of methylene blue (right) and methyl (left). The model of the printed structures is shown in the top right corner of the images.

To better understand the selective adsorption of the individual dyes, we performed an in-depth UV-vis spectroscopy study of the adsorption process, using photo-cross-linked films. After core removal, the porous films were immersed in a dye solution, whose absorption was measured over time. The decrease of the absorption intensity for methylene blue and thioflavin T confirmed the hypothesis that these dyes can be adsorbed in the negatively charges nanopores. In contrast, no evident changes in the UV-vis spectra of methylene orange (of a small size but negatively charged) and rhodamine B (positively charged but of a larger size) were observed, confirming that neither dyes were adsorbed and remained in solution. Additionally, size selectivity was tested by using a binary mixture of methylene blue and rhodamine B (both are cationic dyes). While the intensity of the absorption of the methylene blue solution (with a maximum around a 680 nm wavelength) decreased, the absorption of the rhodamine B solution (with a maximum around a 550 nm wavelength) did not change. This demonstrated the selectivity of the adsorption for methylene blue (Figure 7).

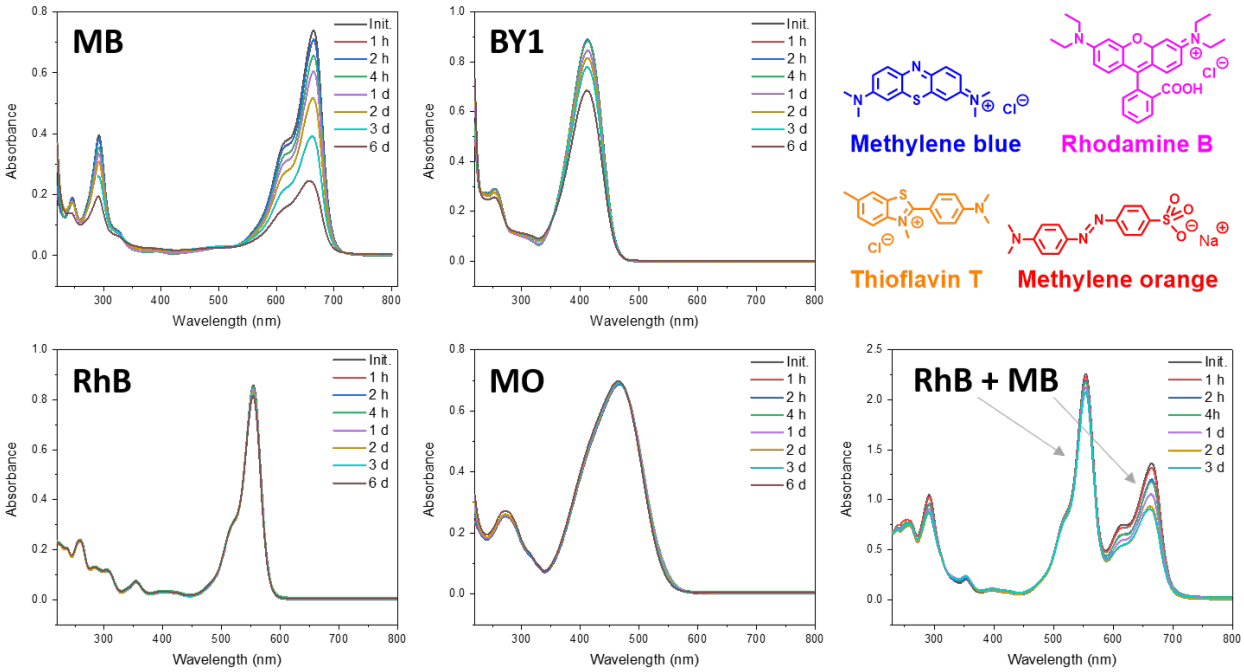

Figure 7. UV-vis study of the adsorption of methylene blue (MB), thioflavin T (BY1), rhodamine B (RhB) and methylene orange (MO) within the pores engendered by the removal of the **TBIB** templating core from a cross-linked film of **TBIB:dA$_3$**.

CONCLUSION

We have demonstrated the successful laser microprinting of a Col$_h$ LC photoresist for the fabrication highly defined porous microstructures for the first time. In particular, we explored hydrogen-bonded 3:1 complexes for this study. It was found that the use of an aromatic core such as **TBIB** was beneficial for the formation of the Col$_h$ mesophase. Thus, the complex **TBIB:dA$_3$** was formulated into a printable photoresist and utilized for the fabrication of 2.5D microprinted structures. Importantly, it was shown that the microprinting of **TBIB:dA$_3$** by two-photon laser printing did not alter the Col$_h$ arrangement of the original material. Moreover, the removal of the central core generated a highly defined nanoporosity of the microprinted material. The selective adsorptive properties of the printed microstructures as well as macroscopic photo-cross-linked

films as references were tested using traceable. The Col_h cross-linked material showed selectivity for small cationic molecules both at the macro- and microscale. Also, WAXS experiments evidenced the retention of the LC order after removal of the template. Although there are still some limitations for the microprinting of complex 3D architectures, this work demonstrates the ability to finely fabricate nanoporous microstructures from Col_h LCs. We believe that this is an important step towards the fabrication of functional porous micro-devices, which can potentially be used for catalysis, filtration, separation, or molecular recognition.

EXPERIMENTAL

Chemical synthesis

The synthesis of **dA**, **TBIB**, **M** and **T** were adapted from previously reported procedures.[63-71] The synthetic procedures and characterizations are detailed in the supplementary information.

The preparation procedures of **TBIB:dA$_3$**, **M:dA$_3$**, **TdA$_3$** were adapted from a reported procedure[56] and are detailed in the supplementary information.

General

^{1}H and ^{13}C NMR experiments were performed using a Bruker Ultrashield plus-500 spectrometer (^{1}H: 500 MHz, ^{13}C: 126 MHz). Chemical shifts are reported in part per million (ppm) and calibrated to the solvent as internal standard. ESI-TOF mass spectrometric data were obtained using a Bruker Daltonics micrOTOF-Q II.

POM

POM was performed using a Leica DMLM HC L35P equipped with an Instec HCS302 heating stage coupled to an Instec mK2000 temperature controller.

Two-photon laser printing

Printing procedure

Two-photon laser printing was performed using a Photonic Professional GT instrument (Nanoscribe GmBH), using a 25×/NA 0.8 objective lens (Zeiss LCI Plan-Neofluar 25×/0.8) in oil-immersion mode. The microprinting was achieved using galvanometer scanners in the xy-plane and using a piezoelectric element in the z-direction. The printing jobs were constructed using a hatching distance of 0.3 μm and a slicing distance of 0.5 μm. If necessary, the printing jobs were split using 250 × 250 × 50 μm^3 rectangular domains. The focal point was manually set at the interface of the photoresist and the glass substrate before each job. The microprinting was achieved using a scanning speed of 25 mm s^{-1} and a laser power of 25 mW, or a scanning speed of 20 mm s^{-1} and a laser power of 20 mW. After microprinting, the microstructures were isolated by development of the sandwich cell in a $CHCl_3$:MeOH mixture.

The printing jobs were computed using DeScribe, and from stl files constructed using Blender.

Sample preparation

A sample of the Col_h photoresist was sandwiched in between two glass slides, using a methacrylate functionalization for the glass slide receiving the printed structures. Prior to printing, the Col_h material was formed by controlled temperature processing using a heating stage, the thickness of the Col_h material was controlled using 4 layers of 16 μm aluminum foil as spacer.

FTIR spectroscopy

FTIR of microstructures

Infrared spectra of the microstructures were taken using an IR microscope (Bruker Hyperion 1000) coupled to a FTIR spectrometer (Bruker Tensor 27) using non-polarized light of a thermal light source. Atmospheric (water vapor and CO_2) absorption was suppressed by purging the whole beam path with dry air. The microstructures were located by means of white light microscopy, and were placed in the center of a circular aperture with a diameter of 105 μm. All spectra were taken

in transmittance geometry with a resolution of 4 cm^{-1} and 100 scans. Relative transmittance spectra were calculated by normalizing the measurements to the transmittance of the bare substrate at a position next to the microstructures.

FTIR of molecular species and polymeric films

FTIR were measured using ATR (iS50 FT-IF, Nicolet). The spectra were measured in a region of 4000 cm^{-1} to 400 cm^{-1} with a resolution of 4 cm^{-1} and 20 scans.

Wide-angle X-Ray scattering

Wide-angle X-ray scattering (WAXS) experiments were performed using a Xeuss 2.0 Q-Xoom (Xenocs SA, Grenoble, France) instrument, equipped with a Genix3D Cu ULC (ultra low divergence) micro focus source of Cu-Kα with an energy of 8.04 keV and a wavelength of 1.5406 Å, and a Pilatus3 R 300K detector (Dectris Ltd., Baden, Switzerland). The non-cross-linked photoresist was placed in a gel-holder, packed between two polyimide foils with a sample thickness of 0.5 mm. Cross-linked films were measured without substrate. The 2D scattering patterns were obtained using a sample to detector distance of 80 mm, resulting in a range of accessible scattering vector (q) from 0.10 to 3.85 $Å^{-1}$. We used an azimuthal integration of the scattering patterns to obtain 1D plots of the intensity I(q) versus q with $q=4\pi\sin(2\theta/2)/\lambda$, where 2θ is the scattering angle and λ is the wavelength of the Cu-Kα source. The measurement time was set to 1800 s and 600 s for the non-cross-linked photoresists and the cross-linked films, respectively. Detailed calculation of the dimensions of the Col_h mesophase are available in the supplementary information.

SEM imaging

The samples, sputter-coated with a 5 nm gold layer, were imaged using a Zeiss Leo 1530 scanning electron microscope operating at 2.0 kV. For volumes visualization, a 45° tilted pin mounts were used.

UV-Vis spectroscopy

UV-vis spectra were recorded on an Agilent Cary 5000 UV-Vis-NIR spectrophotometer.

Fluorescence confocal microscopy

Fluorescent z-stacks of 3D microstructures were carried out on a LSM 980 (Carl Zeiss, Germany) operating in the AiryScan SR-4Y mode. The images were taken using a 20x/0.8 objective. A 639 nm diode laser was used for excitation, and the emission at 670─720 nm was collected.

ASSOCIATED CONTENT

Supporting Information. Detailed materials, methods and synthetic procedures, ^{1}H-NMR and ^{13}C-NMR spectra, ^{1}H-NMR study of the formation of **TBIB:dA$_3$**, FTIR study of the core removal over time, detailed diffractions calculations and summary of results, procedure for the functionalization of glass substrates, additional images of microprinted structures, preparation procedure, POM and WAXS characterization of **M:dA$_3$** and **T:dA$_3$.**

ACKNOWLEDGMENT

The authors acknowledge the Excellence Cluster “3D Matter Made to Order” (EXC-2082/1-390761711) and the Carl Zeiss Foundation through the “Carl-Zeiss-Foundation-Focus@HEiKA”. E.B and M.W. further acknowledge support by the Helmholtz program “Materials Systems Engineering” (MSE) at the Karlsruhe Institute of Technology for general support. The authors also address special thanks to Kai Weißenbruch (Institute of Functional Interfaces, KIT) for the

fluorescence confocal microscopy experiments and to Omar Qaboos Imran and Na Kyung Kim (University of Pennsylvania) for helpful discussions and assistance with the synthesis of TBIB. C. O. and R.D. acknowledge support from NSF through CHE-2124558.

REFERENCES

1. Camposeo, A.; Persano, L.; Farsari, M.; Pisignano, D., Additive Manufacturing: Applications and Directions in Photonics and Optoelectronics. *Advanced optical materials* **2019,** *7* (1), 1800419.
2. Hadibrata, W.; Wei, H.; Krishnaswamy, S.; Aydin, K., Inverse Design and 3D Printing of a Metalens on an Optical Fiber Tip for Direct Laser Lithography. *Nano Letters* **2021,** *21* (6), 2422-2428.
3. Kuang, M.; Wang, J.; Bao, B.; Li, F.; Wang, L.; Jiang, L.; Song, Y., Inkjet Printing Patterned Photonic Crystal Domes for Wide Viewing-Angle Displays by Controlling the Sliding Three Phase Contact Line. *Advanced Optical Materials* **2014,** *2* (1), 34-38.
4. Blachowicz, T.; Ehrmann, G.; Ehrmann, A., Optical Elements from 3D Printed Polymers. *e-Polymers* **2021,** *21* (1), 549-565.
5. Jeong, H. Y.; Lee, E.; An, S.-C.; Lim, Y.; Jun, Y. C., 3D and 4D Printing for Optics and Metaphotonics. *Nanophotonics* **2020,** *9* (5), 1139-1160.
6. Li, J.; Wu, C.; Chu, P. K.; Gelinsky, M., 3D Printing of Hydrogels: Rational Design Strategies and Emerging Biomedical Applications. *Materials Science and Engineering: R: Reports* **2020,** *140*, 100543.
7. Radmanesh, S.; Shabangiz, S.; Koupaei, N.; Hassanzadeh-Tabrizi, S. A., 3D Printed Bio Polymeric Materials as a New Perspective for Wound Dressing and Skin Tissue Engineering Applications: A Review. *Journal of Polymer Research* **2022,** *29* (2), 50.
8. Fricain, J.-C.; De Olivera, H.; Devillard, R.; Kalisky, J.; Rémy, M.; Keriquel, V.; Le Nihounen, D.; Gremare, A.; Guduric, V.; Plaud, A., 3D Bioprinting in Regenerative Medicine and Tissue Engineering. *médecine/sciences* **2017,** *33* (1), 52-59.
9. Baudis, S.; Nehl, F.; Ligon, S. C.; Nigisch, A.; Bergmeister, H.; Bernhard, D.; Stampfl, J.; Liska, R., Elastomeric Degradable Biomaterials by Photopolymerization-Based CAD-CAM for Vascular Tissue Engineering. *Biomedical Materials* **2011,** *6* (5), 055003.
10. Jeong, H. Y.; An, S.-C.; Jun, Y. C., Light Activation of 3D-Printed Structures: from Millimeter to Sub-Micrometer Scale. *Nanophotonics* **2022,** *11* (3), 461-486.
11. Bunea, A.-I.; Martella, D.; Nocentini, S.; Parmeggiani, C.; Taboryski, R.; Wiersma, D. S., Light-Powered Microrobots: Challenges and Opportunities for Hard and Soft Responsive Microswimmers. *Advanced Intelligent Systems* **2021,** *3* (4), 2000256.
12. Decroly, G.; Toncheva, A.; Blanc, L.; Raquez, J.-M.; Lessinnes, T.; Delchambre, A.; Lambert, P., Programmable Stimuli-Responsive Actuators for Complex Motions in Soft Robotics: Concept, Design and Challenges. *Actuators* **2020,** *9* (4), 131.
13. Lao, Z.; Xia, N.; Wang, S.; Xu, T.; Wu, X.; Zhang, L., Tethered and Untethered 3D Microactuators Fabricated by Two-Photon Polymerization: A Review. *Micromachines* **2021,** *12* (4), 465.
14. Ligon, S. C.; Liska, R.; Stampfl, J.; Gurr, M.; Mülhaupt, R., Polymers for 3D Printing and Customized Additive Manufacturing. *Chemical reviews* **2017,** *117* (15), 10212-10290.

15. Ngo, T. D.; Kashani, A.; Imbalzano, G.; Nguyen, K. T.; Hui, D., Additive Manufacturing (3D Printing): A Review of Materials, Methods, Applications and Challenges. *Composites Part B: Engineering* **2018,** *143*, 172-196.
16. Kang, D.-H.; Louis, F.; Liu, H.; Shimoda, H.; Nishiyama, Y.; Nozawa, H.; Kakitani, M.; Takagi, D.; Kasa, D.; Nagamori, E.; Irie, S.; Kitano, S.; Matsusaki, M., Engineered Whole Cut Meat-like Tissue by the Assembly of Cell Fibers Using Tendon-Gel Integrated Bioprinting. *Nature Communications* **2021,** *12* (1), 5059.
17. Kuntanapreeda, S.; Hess, D., Opening Access to Space by Maximizing Utilization of 3D Printing in Launch Vehicle Design and Production. *Applied Science and Engineering Progress* **2021,** *14* (2), 143-145.
18. Subrin, K.; Bressac, T.; Garnier, S.; Ambiehl, A.; Paquet, E.; Furet, B., Improvement of the Mobile Robot Location Dedicated for Habitable House Construction by 3D Printing. *IFAC-PapersOnLine* **2018,** *51* (11), 716-721.
19. Saez, I. M.; Goodby, J. W., Supermolecular Liquid Crystals. *Journal of Materials Chemistry* **2005,** *15* (1), 26-40.
20. Gin, D. L.; Pecinovsky, C. S.; Bara, J. E.; Kerr, R. L., Functional Lyotropic Liquid Crystal Materials. In *Liquid Crystalline Functional Assemblies and Their Supramolecular Structures*, Kato, T., Ed. Springer Berlin Heidelberg: Berlin, Heidelberg, 2008; pp 181-222.
21. Ma, S.; Zhang, Y.; Wang, M.; Liang, Y.; Ren, L.; Ren, L., Recent Progress in 4D Printing of Stimuli-Responsive Polymeric Materials. *Science China Technological Sciences* **2020,** *63* (4), 532-544.
22. Tan, L.; Davis, A. C.; Cappelleri, D. J., Smart Polymers for Microscale Machines. *Advanced Functional Materials* **2021,** *31* (9), 2007125.
23. White, T. J.; Broer, D. J., Programmable and Adaptive Mechanics With Liquid Crystal Polymer Networks and Elastomers. *Nature materials* **2015,** *14* (11), 1087-1098.
24. Roppolo, I.; Chiappone, A.; Angelini, A.; Stassi, S.; Frascella, F.; Pirri, C. F.; Ricciardi, C.; Descrovi, E., 3D Printable Light-Responsive Polymers. *Materials Horizons* **2017,** *4* (3), 396-401.
25. Pozo, M. d.; Sol, J. A. H. P.; van Uden, S. H. P.; Peeketi, A. R.; Lugger, S. J. D.; Annabattula, R. K.; Schenning, A. P. H. J.; Debije, M. G., Patterned Actuators via Direct Ink Writing of Liquid Crystals. *ACS Applied Materials & Interfaces* **2021,** *13* (49), 59381-59391.
26. Ambulo, C. P.; Ford, M. J.; Searles, K.; Majidi, C.; Ware, T. H., 4D-Printable Liquid Metal–Liquid Crystal Elastomer Composites. *ACS Applied Materials & Interfaces* **2021,** *13* (11), 12805-12813.
27. López-Valdeolivas, M.; Liu, D.; Broer, D. J.; Sánchez-Somolinos, C., 4D Printed Actuators With Soft-Robotic Functions. *Macromolecular rapid communications* **2018,** *39* (5), 1700710.
28. Kotikian, A.; Truby, R. L.; Boley, J. W.; White, T. J.; Lewis, J. A., 3D Printing of Liquid Crystal Elastomeric Actuators with Spatially Programed Nematic Order. *Advanced Materials* **2018,** *30* (10), 1706164.
29. Kim, K.; Guo, Y.; Bae, J.; Choi, S.; Song, H. Y.; Park, S.; Hyun, K.; Ahn, S.-K., 4D Printing of Hygroscopic Liquid Crystal Elastomer Actuators. *Small* **2021,** *17* (23), 2100910.
30. Parry, E.; Kim, D.-J.; Castrejón-Pita, A. A.; Elston, S. J.; Morris, S. M., Formation of Radial Aligned and Uniform Nematic Liquid Crystal Droplets via Drop-on-Demand Inkjet Printing into a Partially-Wet Polymer Layer. *Optical Materials* **2018,** *80*, 71-76.

31. Sharma, A.; Hofmann, D.; Hegmann, T., Patterned Alignment of Nematic Liquid Crystals Generated by Inkjet Printing of Gold Nanoparticles and Emissive Carbon Dots on Both Flexible Polymer and Rigid Glass Substrates. *Liquid Crystals* **2016,** *43* (6), 828-838.
32. Spiegel, C. A.; Hippler, M.; Münchinger, A.; Bastmeyer, M.; Barner-Kowollik, C.; Wegener, M.; Blasco, E., 4D Printing at the Microscale. *Advanced Functional Materials* **2020,** *30* (26), 1907615.
33. Carlotti, M.; Mattoli, V., Functional Materials for Two-Photon Polymerization in Microfabrication. *Small* **2019,** *15* (40), 1902687.
34. Martella, D.; Nocentini, S.; Nuzhdin, D.; Parmeggiani, C.; Wiersma, D. S., Photonic Microhand With Autonomous Action. *Advanced Materials* **2017,** *29* (42), 1704047.
35. Nocentini, S.; Riboli, F.; Burresi, M.; Martella, D.; Parmeggiani, C.; Wiersma, D. S., Three-Dimensional Photonic Circuits in Rigid and Soft Polymers Tunable by Light. *ACS Photonics* **2018,** *5* (8), 3222-3230.
36. Tartan, C. C.; Sandford O'Neill, J. J.; Salter, P. S.; Aplinc, J.; Booth, M. J.; Ravnik, M.; Morris, S. M.; Elston, S. J., Read on Demand Images in Laser-Written Polymerizable Liquid Crystal Devices. *Advanced Optical Materials* **2018,** *6* (20), 1800515.
37. Hashemi, S.; Jagodič, U.; Mozaffari, M.; Ejtehadi, M.; Muševič, I.; Ravnik, M., Fractal Nematic Colloids. *Nature communications* **2017,** *8* (1), 1-9.
38. Zeng, H.; Wasylczyk, P.; Parmeggiani, C.; Martella, D.; Burresi, M.; Wiersma, D. S., Light-Fueled Microscopic Walkers. *Advanced Materials* **2015,** *27* (26), 3883-3887.
39. Münchinger, A.; Hahn, V.; Beutel, D.; Woska, S.; Monti, J.; Rockstuhl, C.; Blasco, E.; Wegener, M., Multi-Photon 4D Printing of Complex Liquid Crystalline Microstructures by In Situ Alignment Using Electric Fields. *Advanced Materials Technologies* **2022,** *7* (1), 2100944.
40. Donnio, B.; Guillon, D., Liquid Crystalline Dendrimers and Polypedes. In *Supramolecular Polymers Polymeric Betains Oligomers*, Springer Berlin Heidelberg: Berlin, Heidelberg, 2006; pp 45-155.
41. Shimogaki, T.; Dei, S.; Ohta, K.; Matsumoto, A., Columnar Mesophases Constructed by Hierarchical Self-Organization of Rod-like Diacetylene Molecules. *Journal of Materials Chemistry* **2011,** *21* (29), 10730-10737.
42. Heiney, P. A., Structure and Physical Properties of Columnar Liquid Crystals. In *Handbook of Liquid Crystals*, 2014; pp 1-47.
43. Kaafarani, B. R., Discotic Liquid Crystals for Opto-Electronic Applications. *Chemistry of Materials* **2011,** *23* (3), 378-396.
44. Bhagavath, P.; Shetty, R.; Sunil, D., 1, 3, 5-Triazine-Based Liquid Crystals: An Up-to-Date Appraisal of their Synthetic Design and Mesogenic Properties. *Critical Reviews in Solid State and Materials Sciences* **2020,** *45* (5), 378-409.
45. Han, X.-D.; Tian, X.-L.; Yu, W.-H.; Xiang, S.-K.; Hu, P.; Wang, B.-Q.; Zhao, K.-Q.; Chen, X.-Z.; Feng, C., Influence of Peripheral Alkyl Chain Length on the Mesomorphic Behaviours of Hexasubstituted Triphenylene 2, 3-Dicarboxylic Esters. *Liquid Crystals* **2017,** *44* (11), 1727-1738.
46. Suzuki, Y.; Sakamoto, T.; Yoshio, M.; Kato, T., Development of Functional Nanoporous Membranes Based on Photocleavable Columnar Liquid Crystals – Selective Adsorption of Ionic Dyes. *European Polymer Journal* **2020,** *134*, 109859.
47. Feng, X.; Nejati, S.; Cowan, M. G.; Tousley, M. E.; Wiesenauer, B. R.; Noble, R. D.; Elimelech, M.; Gin, D. L.; Osuji, C. O., Thin Polymer Films with Continuous Vertically Aligned 1 nm Pores Fabricated by Soft Confinement. *ACS Nano* **2016,** *10* (1), 150-158.

48. Liu, S.; Yan, G.; Wang, J.; Zhou, J.; Bie, L.; Jia, Y.; Meng, F., Self-Assembly, Phase Behaviour and Ion-Conducting Property of Pyridinium-Based Ionic Liquid-Crystalline Oligomers. *Liquid Crystals* **2021,** *48* (2), 201-214.
49. Kloos, J.; Joosten, N.; Schenning, A.; Nijmeijer, K., Self-Assembling Liquid Crystals as Building Blocks to Design Nanoporous Membranes Suitable for Molecular Separations. *Journal of Membrane Science* **2021,** *620*, 118849.
50. Devadiga, D.; T.N., A., Liquid Crystal-Based Water Treatment Membranes. *Advanced Materials Interfaces* **2022,** *9* (7), 2101276.
51. Lee, H. K.; Lee, H.; Ko, Y. H.; Chang, Y. J.; Oh, N. K.; Zin, W. C.; Kim, K., Synthesis of a Nanoporous Polymer with Hexagonal Channels From Supramolecular Discotic Liquid Crystals. *Angewandte Chemie* **2001,** *113* (14), 2741-2743.
52. Bögels, G. M.; Lugger, J. A. M.; Goor, O. J. G. M.; Sijbesma, R. P., Size-Selective Binding of Sodium and Potassium Ions in Nanoporous Thin Films of Polymerized Liquid Crystals. *Advanced Functional Materials* **2016,** *26* (44), 8023-8030.
53. Lugger, J. A.; Mulder, D. J.; Bhattacharjee, S.; Sijbesma, R. P., Homeotropic Self-Alignment of Discotic Liquid Crystals for Nanoporous Polymer Films. *ACS Nano* **2018,** *12* (7), 6714-6724.
54. Lugger, J. A. M.; Marín San Román, P. P.; Kroonen, C. C. E.; Sijbesma, R. P., Nanoporous Films with Photoswitchable Absorption Kinetics Based on Polymerizable Columnar Discotic Liquid Crystals. *ACS Applied Materials & Interfaces* **2021,** *13* (3), 4385-4392.
55. Feng, X.; Kawabata, K.; Kaufman, G.; Elimelech, M.; Osuji, C. O., Highly Selective Vertically Aligned Nanopores in Sustainably Derived Polymer Membranes by Molecular Templating. *ACS Nano* **2017,** *11* (4), 3911-3921.
56. Imran, O. Q.; Kim, N. K.; Bodkin, L. N.; Dwulet, G. E.; Feng, X.; Kawabata, K.; Elimelech, M.; Gin, D. L.; Osuji, C. O., Nanoscale Thickness Control of Nanoporous Films Derived from Directionally Photopolymerized Mesophases. *Advanced Materials Interfaces* **2021,** *8* (5), 2001977.
57. Feng, X.; Kawabata, K.; Cowan, M. G.; Dwulet, G. E.; Toth, K.; Sixdenier, L.; Haji-Akbari, A.; Noble, R. D.; Elimelech, M.; Gin, D. L., Single Crystal Texture by Directed Molecular Self-Assembly Along Dual Axes. *Nature materials* **2019,** *18* (11), 1235-1243.
58. Concellón, A.; Schenning, A. P.; Romero, P.; Marcos, M.; Serrano, J. L., Size-Selective Adsorption in Nanoporous Polymers From Coumarin Photo-Cross-Linked Columnar Liquid Crystals. *Macromolecules* **2018,** *51* (6), 2349-2358.
59. Gracia, I.; Romero, P.; Serrano, J. L.; Barberá, J.; Omenat, A., Templated Nanoporous Membranes Based on Hierarchically Self-Assembled Materials. *Journal of Materials Chemistry C* **2017,** *5* (8), 2033-2042.
60. Marin San Roman, P.; Nijmeijer, K.; Sijbesma, R. P., Sulfonated Polymerized Liquid Crystal Nanoporous Membranes for Water Purification. *Journal of Membrane Science* **2022,** *644*, 120097.
61. Xiao, A.-Q.; Lyu, X.-L.; Pan, H.-B.; Tang, Z.-H.; Zhang, W.; Shen, Z.-H.; Fan, X.-H., Homeotropic Alignment and Selective Adsorption of Nanoporous Polymer Film Polymerized from Hydrogen-bonded Liquid Crystal. *Chinese Journal of Polymer Science* **2020,** *38* (11), 1185-1191.
62. Li, C.; Cho, J.; Yamada, K.; Hashizume, D.; Araoka, F.; Takezoe, H.; Aida, T.; Ishida, Y., Macroscopic ordering of helical pores for arraying guest molecules noncentrosymmetrically. *Nature communications* **2015,** *6* (1), 1-10.

63. Smith, R. C.; Fischer, W. M.; Gin, D. L., Ordered Poly(p-phenylenevinylene) Matrix Nanocomposites via Lyotropic Liquid-Crystalline Monomers. *Journal of the American Chemical Society* **1997,** *119* (17), 4092-4093.
64. Ding, J. H.; Gin, D. L., Catalytic Pd Nanoparticles Synthesized Using a Lyotropic Liquid Crystal Polymer Template. *Chemistry of materials* **2000,** *12* (1), 22-24.
65. Barberá, J.; Puig, L.; Romero, P.; Serrano, J. L.; Sierra, T., Propeller-like Hydrogen-Bonded Banana−Melamine Complexes Inducing Helical Supramolecular Organizations. *Journal of the American Chemical Society* **2006,** *128* (13), 4487-4492.
66. Feringán, B.; Romero, P.; Serrano, J. L.; Giménez, R.; Sierra, T., Supramolecular Columnar Liquid Crystals Formed by Hydrogen Bonding between a Clicked Star-Shaped s-Triazine and Benzoic Acids. *Chemistry – A European Journal* **2015,** *21* (24), 8859-8866.
67. King, A. O.; Negishi, E.; Villani Jr, F. J.; Silveira Jr, A., A General Synthesis of Terminal and Internal Arylalkynes by the Palladium-Catalyzed Reaction of Alkynylzinc Reagents with Aryl Halides. *The Journal of Organic Chemistry* **1978,** *43* (2), 358-360.
68. Sonoda, M.; Inaba, A.; Itahashi, K.; Tobe, Y., Synthesis of Differentially Substituted Hexaethynylbenzenes Based on Tandem Sonogashira and Negishi Cross-Coupling Reactions. *Organic letters* **2001,** *3* (15), 2419-2421.
69. Shimada, K.; Sugawara, A.; Korenaga, T.; Kawashima, H., Total Synthesis and Structural Elucidation of Two Unusual Non-Methylene-Interrupted Fatty Acids in Ovaries of the Limpet Cellana Toreuma. *Lipids* **2017,** *52* (12), 1019-1032.
70. Kelly, S. M., Ferroelectric Liquid Crystals. Part 9. Laterally Substituted Phenyl Benzoates Incorporating a trans-1,4-Disubstituted Cyclohexane Ring. *Helvetica Chimica Acta* **1989,** *72* (3), 594-607.
71. Beginn, U.; Zipp, G.; Möller, M., Synthesis and Characterization of Tris-Methacrylated 3,4,5-Tris[(alkoxy)benzyloxy]benzoate Derivatives. *Chemistry – A European Journal* **2000,** *6* (11), 2016-2023.